

# AN EXPLANATION FOR THE SLOW AND UNIFORM ROTATION OF THE SOLAR CORE

R. Arlt and G. Rüdiger

Astrophysikalisches Institut Potsdam, An der Sternwarte 16, D-14482 Potsdam, Germany

## ABSTRACT

The radiative core of the Sun appears to rotate uniformly and as slowly as the surface. The young Sun was a fast rotator and fully convective in the T Tauri phase. Magnetic winds can slow down the surface of the star but viscous stresses are too small to affect the stellar core thus leading to strong differential rotation. Also convection efficiently builds up differential rotation at any time of the Sun's life, and the entire star should have exhibited a non-uniform rotation profile. As convection ceased in the core, the radiative zone is left with microscopic viscosity which cannot damp differential rotation during the life-time of the Sun. We study the question why the solar radiation zone is both a slow and uniform rotator. We present magnetohydrodynamic simulations of the decay of the differential rotation profile in the radiative core due to magnetorotational instability. Unstable modes grow fast, and resulting flows equalize the rotation profile. We estimate that the decay time of the differential rotation is about 100 million years.

Key words: Solar rotation; MHD; instabilities.

## 1. MOTIVATION

The exploration of the solar structure by helioseismology led to a latitudinal differential rotation in the convection zone, an amazingly uniform rotation in the radiative core, and a thin transition where largest radial gradients of angular velocity occur.

The observations of young stars show that objects with solar masses have rotational periods of a few days. The spin-down of solar-type stars was investigated by Stępień (1988). The spin-down is attributed to magnetic breaking through thermal winds. Figure 1 shows the rotation rate as a function of time as obtained in the aforementioned paper. This mechanism is certainly efficient to take away angular momentum *from the surface* of the star, but we are left with the question how the inner parts of the object get rid of its short rotation period.

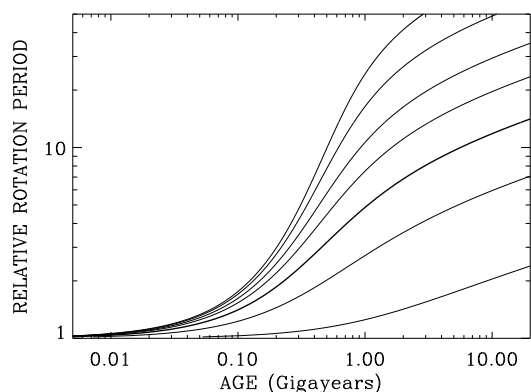


Figure 1. Evolution of the surface rotation period from an initially fast rotation by breaking with thermal winds after Stępień (1988). The various lines emerge from a free parameter involving the field geometry and initial rotation period (actually the Rossby number). The Sun and various measurements from open stellar clusters with known ages are fit excellently by the thick line.

The turbulence of the fully convective stage of evolution may be a transporter of angular momentum, but numerical simulations in accretion disks could not yet show outward transport of angular momentum by convection (e.g. Stone & Balbus 1996). As convection ceases in the core of the young main-sequence object, we are left with microscopic viscosity of the gas anyway. We can estimate the time-scale of viscous decrease of the rotation in case of external breaking simply by estimating the time-scale due to the gas' viscosity of roughly  $\nu = 10 \text{ cm}^2/\text{s}$ . For a core radius of  $R = 10^{10} \text{ cm}$ , we get a viscous time-scale of  $R^2/\nu \approx 10^{11} \text{ yr}$  which is an order of magnitude more than the full life-time of the Sun. Viscous decay of the differential rotation of the largest layer of the solar interior is thus not applicable. *How can the solar core ever "feel" the spin-down of the outer layers from 2 to 25 days period?*

Moreover, differential rotation of the core should be a left-over from convection. The differential rotation of the convection zone is a consequence of the convection itself (Küker et al. 1996) which is driven by the

internal heat source and maintains a non-uniform rotation. The very young Sun in its pre-main-sequence phase was fully convective and must have built up a rotation profile which was differential at nearly all radii (Küker & Stix 2001).

It is thus justified to assume that the young Sun exhibited a fully differential rotation at all radii at the moment when the radiative core “cleared up”. We are thus in need to explain *why the solar core is a slow and uniform rotator*.

The combination of differential rotation and a weak magnetic field provides a fast instability (Balbus & Hawley 1991). The instability has turned out to be an efficient generator of turbulence in accretion disks, but is as well applicable to a stellar interior as long as the angular velocity decreases with axis distance in parts of the spherical domain. The mechanism is typically termed magneto-rotational instability or Balbus-Hawley instability. It is a consequence of the local and linear MHD equations; a lower limit to the magnetic field is only imposed by the magnetic diffusivity  $\eta$  which is extremely small for stellar plasmas. Field geometry is also almost irrelevant for the onset of the instability. The magneto-rotational instability is hence most likely to occur in stellar radiative zones as soon as differential rotation emerges.

We present numerical simulations of the MHD equations in Boussinesq approximation which show the fast onset of instability and the decay of differential rotation towards a uniform angular velocity. The following Section gives an overview of the numerical setup, and Section 3 deals with the results, the time-scales of differential-rotation decay in particular.

## 2. NUMERICAL 3D-SIMULATIONS

A three-dimensional spectral MHD code in spherical coordinates was developed by Hollerbach (2000) and applied to our specific problem. The computational domain covers a full spherical shell from  $r_i = 0.13$  to  $r_o = 0.65$  if scaled to the present solar core. The full angular extents in colatitude and longitude is considered ( $\theta = [0, \pi]$  and  $\phi = [0, 2\pi]$  resp.). The time-dependent, non-dimensionalized MHD equations are

$$\begin{aligned} \left(\frac{\partial}{\partial t} + \vec{u} \cdot \nabla\right) \vec{u} &= -\nabla p + \text{Pm} \nabla^2 \vec{u} \\ &\quad + (\nabla \times \vec{B}) \times \vec{B} \quad (1) \\ \frac{\partial \vec{B}}{\partial t} &= \nabla^2 \vec{B} + \nabla \times (\vec{u} \times \vec{B}) \quad (2) \end{aligned}$$

where  $\vec{u}$  is the velocity,  $\vec{B}$  is the magnetic field, and  $p$  is the pressure which is not explicitly calculated in this model, but eliminated by applying the curl-operator in Equation (1). Lengths are normalized by  $R_\odot$ , times by  $R_\odot^2/\eta$ , thus velocities by  $\eta/R_\odot$  and magnetic fields by  $\sqrt{\mu_0 \rho_0 \eta}/R_\odot$ . Note that permeability  $\mu_0$  and density  $\rho_0$  are constants in our approach.

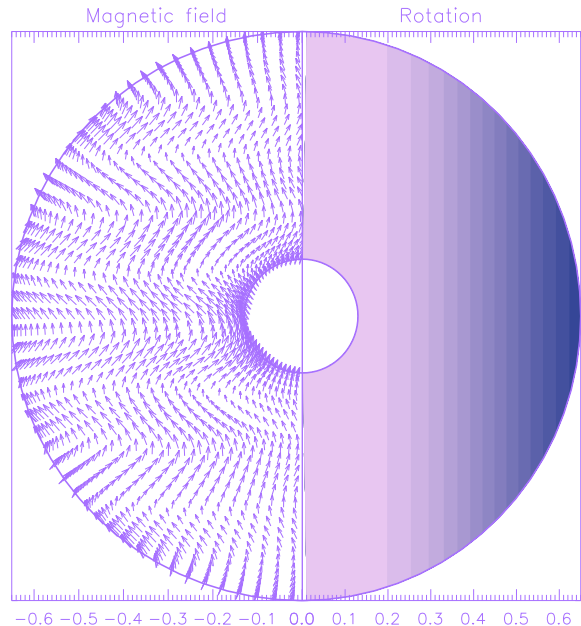


Figure 2. Vertical cut through the initial configuration of the simulations. The magnetic field is vertical with a horizontal wave perturbation which is not symmetric with respect to the equator and non-axisymmetric (LEFT). The initial velocity field is purely azimuthal depending on the axis distance only (RIGHT).

In fact, the velocity and magnetic field are represented by potentials, each of them being decomposed in Chebyshev polynomials (radial direction), Legendre polynomials (latitudinal direction), and Fourier modes (azimuthal direction), i.e.

$$\vec{u} = \nabla \times (e\vec{r}) + \nabla \times \nabla \times (f\vec{r}), \quad (3)$$

$$\vec{B} = \nabla \times (g\vec{r}) + \nabla \times \nabla \times (h\vec{r}), \quad (4)$$

where  $\vec{r}$  is the unit vector in radial direction, and

$$\begin{aligned} e(r, \theta, \phi) &= \sum_{k=1}^K \sum_{l \geq m=0}^L \sum_{m=0}^M T_{k-1}(x) P_l^m(\cos \theta) \\ &\quad \left[ e_{klm}^{(c)} \cos(m\phi) + e_{klm}^{(s)} \sin(m\phi) \right] \quad (5) \end{aligned}$$

etc. for the other potentials  $f$ ,  $g$ , and  $h$ , with

$$r = \frac{r_o + r_i}{2} + \frac{r_o - r_i}{2} x \quad (6)$$

transforming the radial extent of the computational domain between  $r_i$  and  $r_o$  to the standard interval  $(-1, 1)$  of the Chebyshev polynomials. The representation by potentials implies that  $\nabla \cdot \vec{u} = 0$  and  $\nabla \cdot \vec{B} = 0$  are always fulfilled exactly. The six sets of spectral coefficients  $e_{klm}^{(c)}$ ,  $e_{klm}^{(s)}$ ,  $\dots$ ,  $h_{klm}^{(s)}$  are integrated with a predictor-corrector time-stepping of second order where the diffusive terms are treated implicitly.

The magnetic Prandtl number  $\text{Pm}$  is the ratio of gas viscosity and magnetic diffusivity. Stellar gases

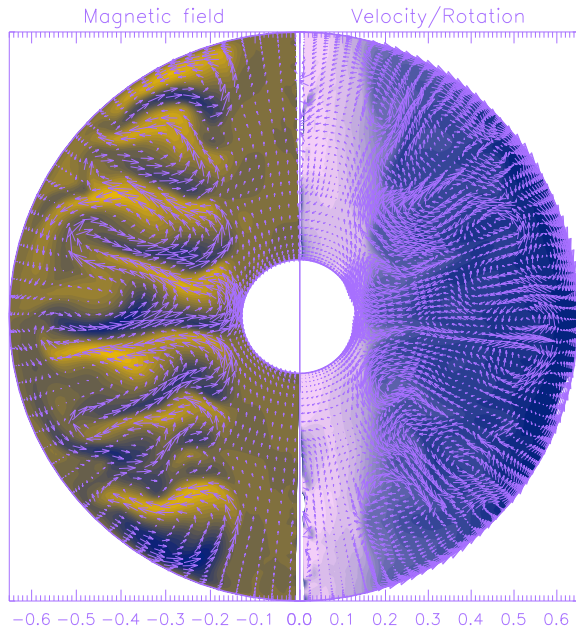


Figure 3. Vertical cut through magnetic field (LEFT) and velocity field (RIGHT) after 4.8 rotation periods near the axis. The grey levels of the velocity plot represent the angular velocity, not the azimuthal velocity.

possess magnetic Prandtl numbers of  $Pm \approx 0.01$ . Values different from unity are typically difficult to achieve by numerical schemes. Values vastly different from unity mean that the time-scales for the diffusive processes in velocity and magnetic fields differ very much and are thus hard to cover appropriately by one simulation.

The initial conditions for the velocity imply the second free parameter, since the MHD evolution is subject to a differential rotation which in our case just depends on the axis distance

$$\Omega(r \sin \theta) = \Omega_0 / \sqrt{1 + (2r \sin \theta)^{2q}}. \quad (7)$$

The parameter  $\Omega_0$  is, when normalized, a magnetic Reynolds number of the system,  $Rm = R^2 \Omega_0 / \eta$ . The steepness of the rotation profile is given by  $q = 2$  in the beginning. Such a profile was intentionally chosen since it is hydrodynamically stable in the entire sphere (apart from slow viscous decay). The two free parameters  $Pm$  and  $Rm$  are varied in our simulations. The initial magnetic field is a homogeneous vertical field plus a wave-like perturbation as a Fourier mode  $m = 1$ . The field is not symmetric with respect to the equator and not axisymmetric, and nonlinear coupling may excite all spectral modes integrated here. The initial conditions are graphically shown in Figure 2.

The inner boundary  $r_i > 0$  is not motivated physically, but required by the numerical approach used for the simulations. The flow at the two radial boundaries is stress-free, i.e. the corresponding conditions  $u_r = 0$ ,  $\partial(u_\theta/r)/\partial r = 0$ , and  $\partial(u_\phi/r)/\partial r = 0$  are converted into conditions for the potentials and

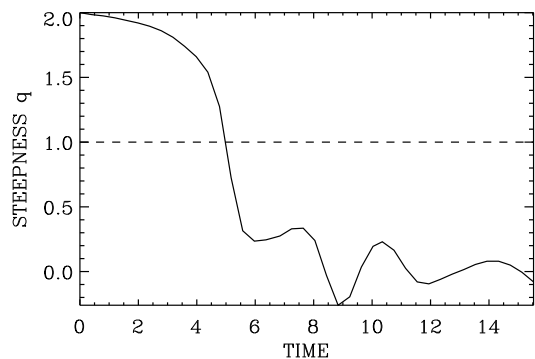


Figure 4. Variation of the steepness of the rotation profile with time as computed from azimuthal averages of the angular velocity of the model with  $Rm = 10000$ . The resulting function of  $r$  was fitted to a function of the form (7). The dotted line indicates  $q = 1$  which will be used to define the decay time of the differential rotation.

imposed on the integration at  $r_i$  and  $r_o$ . The magnetic fields is supposed to be a vacuum field below  $r_i$  and above  $r_o$ . The actual condition  $\nabla \times \vec{B} = \vec{0}$  translates to very simple boundary conditions in the setup of the above potentials with decomposition into spherical harmonics.

The truncation of the spectral decomposition is at 50 Chebyshev polynomials, 100 Legendre polynomials, and 30 Fourier modes,  $(K, L, M) = (50, 100, 30)$ . This corresponds to a resolution in real space of about  $100 \times 152 \times 46$  grid points. The nonlinear terms  $-(\vec{u} \cdot \nabla)\vec{u} + (\nabla \times \vec{B}) \times \vec{B}$  and  $\nabla \times (\vec{u} \times \vec{B})$  are computed in real space and the spectral decomposition of these “right sides” are fed into the implicit predictor-corrector scheme of the linear part of Equations (1) and (2). First simulations with lower resolutions of  $(K, L, M) = (25, 30, 30)$  and  $(K, L, M) = (50, 50, 30)$  led to the same results within 3%.

### 3. RESULTS

Our simulations provide decay times of the differential rotation profile (7). We measure the time until the  $\Omega$ -profile reaches a given average gradient which is measured in the equatorial plane. The first rotations of the object show the onset of the magneto-rotational instability as expected from linear analysis (Kitchatinov & Rüdiger 1997) and simulations of accretion disks (Arlt & Rüdiger 2001). A snapshot of this situation is shown in Figure 3. Radial velocities emerge and give rise to angular-momentum redistribution with a net effect towards larger axis distances. The flow does not become unstable near the axis where differential rotation is negligible.

The decay of the rotation profile by kinetic and magnetic angular momentum transport is measured in terms of the steepness  $q$  of the differential rotation as

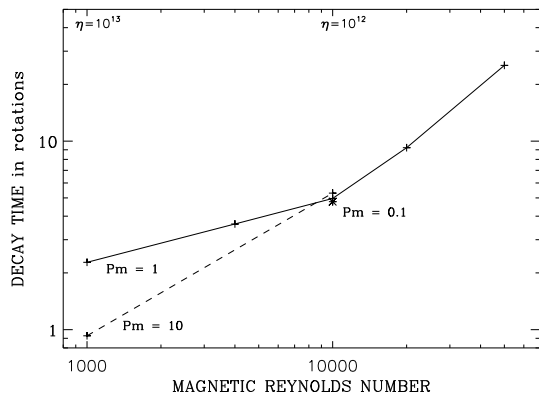


Figure 5. Decay time of the differential rotation measured in rotational periods. If we fix a certain rotation period, the magnetic Reynolds number  $Rm$  is a measure for the diffusivity  $\eta$ . The solid line gives the results for  $Pm = 1$ , the dashed line for  $Pm = 10$ ; a single simulation was achieved for  $Pm = 0.1$  as shown by the asterisk.

used in the initial condition (7). We use the spatial reconstruction of the velocity and average the angular velocity  $u_\phi/r \sin \theta$  azimuthally for each radial grid zone. For simplicity only the equatorial plane is used providing 46 points for the averages. We obtain a one-dimensional function  $\Omega(r \sin \theta)$  and fit a profile of the form (7) with two free parameters,  $\Omega_0$  and  $q$ . The temporal development of the steepness  $q$  is plotted in Figure 4. In the following we will use the time to reach  $q = 1$  as the definition of a decay time  $\tau_{\text{decay}}$  of the differential rotation.

At present, the physical properties of the Sun are not yet accessible by computer simulations, and compromises in the free parameters are the prerequisite for any numerical study. The magnetic Reynolds number of the Sun is of the order of  $10^{13}$ , and the magnetic Prandtl number is perhaps  $Pm = 0.01$ . Equations with these values are hard to integrate numerically. We choose various  $Rm$  from 1000 to 50000 in order to obtain a general trend in the decay times. Figure 5 shows the results for a set of  $Rm$  and  $Pm$ . We found no significant dependence of the decay times on  $Pm$  which is a numerical fortune. We assume that the rotation period of the early Sun is given and vary the magnetic diffusivity. The decay time is measured in rotation times. The graph shows a tendency of a power-law at high Reynolds numbers, such as

$$\frac{\tau_{\text{decay}}}{\tau_{\text{rot}}} = \frac{Rm}{2 \cdot 10^3} \quad (8)$$

When comparing the results with real characteristics of the Sun at an age of say 100 Myr, we may assume a rotation period of 5 days giving  $\Omega = 10^{-5} \text{ s}^{-1}$ . The radius of the early radiative core may be assumed to be roughly  $R = 0.5R_\odot = 4 \cdot 10^{10} \text{ cm}$ . A magnetic Reynolds number of 10000 as shown in Figure 5 corresponds to a diffusivity of  $\eta = 10^{12} \text{ cm}^2/\text{s}$ . Equa-

tion (8) may in fact be converted to diffusion times  $\tau_{\text{diff}} = R_\odot^2/\eta$ , such that  $\tau_{\text{decay}} \approx 10^{-2}\tau_{\text{diff}}$ .

An extrapolation of the decay times to the solar  $Rm$  of  $10^{13}$  yields  $\tau_{\text{decay}} \approx 10^8 \text{ yr}$ . The Sun is more than an order of magnitude older, thus showing a uniformly rotating radiative core. We conclude that the process of the magneto-rotational instability provides a sufficiently fast mechanism to generate turbulent diffusion. The complex flow emerging is capable of reducing the differential rotation of the radiative zone on a very suitable time-scale. The extrapolation spans several orders of magnitude, but since the magneto-rotational instability has proved to be robust against broad parameter variations, we feel confident that this mechanism is at work in radiative zones. The instability produces a turbulence which is an efficient transporter of angular momentum outwards. This has already been shown and was necessary for accretion disk.

The spin-down is actually an ongoing process due to loss of angular momentum by the solar wind. The mechanism presented here is likely to act at any time a radiative core is present. The turbulent flows will not be as violent as shown in our initial-condition model. It will rather redistribute angular momentum continuously which is not achieved by viscous stresses of the plasma.

The process of equalization of the rotation profile also implies a growth of the magnetic energy. Since a possible dynamo will rely here on a differential rotation profile, it will die out as soon as the gradients in the rotation profile vanish. In our model, there is no replenishing mechanism of differential rotation at the outer boundary (e.g. by convection). This is why we cannot give statements about dynamo action in a radiative zone.

## ACKNOWLEDGMENTS

The present work has greatly benefited from the collaboration with Rainer Hollerbach to whom we express our gratitude.

## REFERENCES

- Arlt R., Rüdiger G., 2001, A&A 374, 1035
- Balbus S.A., Hawley J.F., 1991, ApJ 376, 214
- Hollerbach R., 2000, Int. J. Num. Meth. Fluids 32, 773
- Kitchatinov L.L., Rüdiger G., 1997, MNRAS 286, 757
- Küker M., Rüdiger G., Pipin V.V., 1996, A&A 312, 615
- Küker M., Stix M., 2001, A&A 366, 668
- Stępień K., 1988, ApJ 335, 907
- Stone J.M., Balbus S.A., 1996, ApJ 464, 346